COMPUTER BASED DIAGNOSIS SYSTEM OF THYROID NODULES FROM SCINTIGRAPHIC IMAGES

(SİNTİGRAFİ GÖRÜNTÜLERİNDEN TİROİD NODÜLLERİNİN BİLGİSAYAR DESTEKLİ TANI SİSTEMİ)

by

AYSUN SEZER, B.S.

Thesis

Submitted in Partial Fulfillment

of the Requirements

for the Degree of

MASTER OF SCIENCE

in

INDUSTRIAL ENGINEERING

in the

GRADUATE SCHOOL OF SCIENCE AND ENGINEERING

of

GALATASARAY UNIVERSITY

September 2019

This is to certify that the thesis entitled

COMPUTER BASED DIAGNOSIS SYSTEM OF THYROID NODULES FROM SCINTIGRAPHIC IMAGES

prepared by **AYSUN SEZER** in partial fulfillment of the requirements for the degree of **Master of Science in Industrial Engineering Department** at the **Galatasaray University** is approved by the

Examining Committee:

Assoc. Prof. Dr. S. EMRE ALPTEKIN
Supervisor, **Industrial Engineering Department, GSU** _____

Assoc. Prof. Dr. MÜJDE GENEVOIS
Industrial Engineering Department, GSU _____

Assoc. Prof. Dr. SEDA YANIK ÖZBAY
Industrial Engineering Department, ITU _____

Date: _____

ACKNOWLEDGMENTS

Firstly, I would like to express my sincere gratitude to my advisor Assoc. Prof. Dr. S. Emre ALPTEKIN for the continuous support of my thesis, for his patience, motivation, and immense knowledge. His guidance helped me allthrough my research and writing of this thesis.

I would like to thank the rest of my thesis committee for their insightful comments and encouragement. My sincere thanks also goes to Dr.Hasan Basri Sezer, who provided me an opportunity to collect data, and research facilities.

TABLE OF CONTENTS

LIST OF FIGURES

LIST OF TABLES

ABSTRACT

In Modern medicine, segmentation of anatomical regions and automatic classification of diseases using various medical images plays a major role in diagnosis and treatment of disease. Scintigraphic imaging is one of the accepted imaging modalities for diagnosis of thyroid gland disorders. In our study, the speckle noise was reduced in the scintigraphic images with the optimized Bayesian non-local averaging filter. The thyroid gland is automatically segmented by local-based active contour method and the thyroid gland pathologies were classified with convolutional artificial neural networks, one of the deep learning methods. The proposed computer based diagnosis system is compared with Pyramid of Histograms of Orientation Gradients, Gray Level Co-occurrence Matrix, Local Configuration Pattern and Bag of Feature methods. In this study, the common pathological patterns of scintigraphic images of the thyroid gland were successfully classified by CNN with an average of 94%.

Keywords : Deep Learning, Image Classification, Active Contour, Noise Reduction, Thyroid Nodules

RÉSUMÉ

En médecine moderne, la segmentation des régions anatomiques et la classification automatique des maladies à l'aide de diverses images médicales jouent un rôle majeur dans le diagnostic et le traitement de la maladie. L'imagerie scintigraphique est l'une des modalités d'imagerie acceptées pour le diagnostic des troubles de la glande thyroïde. Dans notre étude, le bruit de speckle a été réduit dans les images scintigraphiques avec le filtre bayésien non local moyen. La glande thyroïde est automatiquement segmentée par la méthode du contour actif local et les pathologies de la glande thyroïde ont été classées avec des réseaux de neurones artificiels convolutifs, l'une des méthodes d'apprentissage en profondeur. Le système de diagnostic informatisé proposé est comparé à la pyramide d'histogrammes de gradients d'orientation, à la matrice de cooccurrence au niveau de gris, au modèle de configuration locale et au sac de caractéristiques. Dans cette étude, les profils pathologiques communs des images scintigraphiques de la glande thyroïde ont été classés avec succès par CNN avec une moyenne de 94%.

Mots Clés : Apprentissage en Profondeur, Classification des Images, Contour Actif, Nodules Thyroïdiens à Réduction de Bruit

ÖZET

Modern tıpta çeşitli tıbbi görüntüler kullanılarak anatomik bölgelerin bölütlenmesi ve hastalıkların otomatik olarak sınıflandırılması hastalık teşhis ve tedavisinde büyük rol oynamaktadır. Tiroid gland bozukluklarında sintigrafi görüntüleri tanı için kabul gören görüntüleme yöntemlerinden biridir. Çalışmamızda sintigrafi görüntülerinde bulunan benek gürültüsü optimize edilmiş Bayesian yerel olmayan ortalama filtre ile giderilmiştir. Tiroid bezi bölgesi lokal tabanlı aktif kontur metodu ile otomatik olarak bölütlendirilerek derin öğrenme metodlarından biri olan evrişimsel yapay sinir ağları ile tiroid bezi patolojileri otomatik olarak sınıflandırılmıştır. Önerilen bilgisayar tabanlı tedavi sistemi Yönelim Derecelerinin Histogram Piramidi, Gri Düzeyli Eş-Olma Matrisi, Yerel Yapılandırma Deseni ve Özellik Çanta Yöntemleri ile karşılaştırılmıştır. Bu çalışmada, tiroid bezinin sintigrafik görüntülerinin yaygın patolojik paternleri önerilen CNN tarafından %94 ortalama başarıyla sınıflandırılmıştır.

Anahtar Kelimeler : Derin Öğrenme, Görüntü Sınıflandırma, Aktif Kontur, Gürültü Azaltma, Tiroid Nodülleri

1 INTRODUCTION

Computer aided decision making systems are useful tools for clinicians in evaluation and measurement of medical images to help diagnosis of many conditions. Automatic segmentation of thyroid nodules from scintigraphic images and determination of type of nodules may improve the evaluation performance. We conducted an extensive literature search on computer aided systems to help diagnosis of thyroid nodules, nevertheless we could not encounter any computer based diagnosis system which automatically segment scintigraphic images and classify thyroid nodules based on CNN as diffuse homogeneous uptake, diffuse non-homogeneous uptake, hyperactive nodule, hypoactive nodule and multinodular uptake. There are scarce studies with limited value which achieved segmentation of only some anatomic structures in the ultrasound images.

Scintigraphy is a procedure that produces pictures of anatomical structures based on the behavior of the target tissue. After administration of intravenous fluids which contain targeted radioisotopes (gamma emitter of a short half-life) the selective uptake of the target tissue is determined by scanning the body with a special device to represent the distribution of it. This visual display of the functional tissue is used to diagnose, stage, and monitor diseases, especially tumoral conditions. Thyroid tissue has a great affinity to Iodine. Therefore in thyroid scintigraphy radio-iodine is used to provide information regarding both thyroid anatomy and physiology and can play an integral role in the diagnosis and management of thyroid pathologies.

Computer based recognition and classification of medical images is a popular approach to diagnosis of several disease conditions. Nevertheless, many computer aided dagnosis (CAD) systems are still based on handcrafted methods. This approach mainly depends on experience of the evaluator and the selection of efficient multiscale geometric analysis algorithm to obtain desired shape and texture features. Curvelet, contourlet and shearlet transforms are well known algorithms which may provide satisfactory extraction of shape and texture features. Because translation of image by those methods into another domain may gives very powerful texture and shape features. Even so all of these approaches require prior knowledge of the designer for the feature extraction and selection (heuristic and mathematical). The new era in the computer perception is evolving by the introduction of deep learning methods which extract discriminative features from the data by using machine learning approaches.

Many medical CAD systems in the literature are based on classification of extracted texture and shape features from different imaging modalities.

There are studies which proved that the success rates of the proposed CAD systems increase when the shape and texture features were extracted from coefficients of transformations like shearlet, curvelet etc. However this handcrafted texture and shape feature extraction approach is somewhat heuristic of which the success of the system depends basically on the insight and experience of the researchers. Therefore the sensitivity and specificity rates of many of these proposed systems are not in the desired limits for them to be employed in the clinical fields.

Feature extraction from the coefficients of transformations is proven to increase the success rates of the proposed CAD system. This heuristic approach is, not surprisingly, dependent on the training level and insight of the researchers. Many of the proposed CAD systems, therefore, provide results that are below the desired levels for clinical application. This limitation was achieved with the successful design of the imitation mechanism of the vertebrate visual cortex. This alternative approach to the processing of images by artificial intelligence is an imitation of the methods of perception and analysis inherited from nature. The deep neural network is a popular self-learning approach used to recognize the texture and shape characteristics of an image by processing them across multiple layers of virtual neurons.

Deep CNNs may be regarded as the new era in the medical image segmentation. Their enormous architectural versatility provides extraction of discriminative texture and shape features in a great variety of medical problems. Adjusting the architecture of CNN to create a shallow network increases its capacity to extract low level features like edges. Deeper network architectures are more suitable for extraction of high level features like shape information. Increasing the number of the layers in a CNN increases its capacity to learn more complex image features. The great capacity of CNNs in object recognition, image segmentation and classification with relatively small amount of training data are essential characteristics required in the medical diagnosis field. This thesis proposes a CAD system to overcome the speckle noise of the scintigraphic images which deteriorates determination of anatomical structures. Speckle is a granular interference that inherently exists in ultrasound, scintigraphic and synthetic aperture radar (SAR) images. Reducing speckle noise provide to better visualization of image and increase the performance of the image processing algorithm to recognize an object

or segmentation of region interest.

Selection of a successful noise reduction method to overcome the speckle noise problem in the scintigraphic images and preservation of critical anatomical structures in the image during the noise reduction process are vital in order to get prospering results. Since both visual and automatic segmentation depends on clearly distinguishable representation of the vital anatomical structures in the image. We applied optimized Bayesian non-local mean (OBNLM) filter which is stated to be one of the powerful speckle noise reduction methods in ultrasound images (Coupé et al., 2009). Decreasing the speckle noise by preserving edge information based on OBNLM method is the important step of our proposed CAD system.

Another important step of our CNN based CAD system is the production of adequate size image patches from the desired localization. An ideal image patch is the one which contains all important anatomical structures but not irrelevant tissues which may hamper the classification result. In this study the Statistical level set method which is one of the successful local region based active contours models for segmentation of inhomogeneous and noisy images was employed to segment necessary anatomical area (Zhang, Zhang, Lam and Zhang, 2016). By this way we obtained images patches for diffuse homogeneous uptake, diffuse non-homogeneous uptake, hyperactive nodule, hypoactive nodule and multinodular uptake. Defined region of interest (ROI) were used to feed our proposed CNN. Proposed CNN architecture provide to extract discriminative features of the thyroid nodules in the defined ROI of scintigraphic images and classified thyroid diseases.

CNNs consist of 4 types of layers as convolutional, activation, pooling and fully connected, each of which has a different role to complete the desired mission. Like the receptive field of a human retinal neuron, gathered information from each neuron represents a specific local area of the image which overlaps with others creating a better representation of an image in the convolutional layer. The convolutional layer creates feature maps according to the weights of the neuronal inputs in which the shared weights constitute a filter for each map. Through these feature maps the efficacy of the convolutional layer increases and the over-fitting is prevented. The activation layer follows the convolutional layer. The nonlinear property of the activation layer is required for extraction of more complex features from the input signals generated by the convolutional layer. The pooling layer is the next layer which statistically analyses the inputs

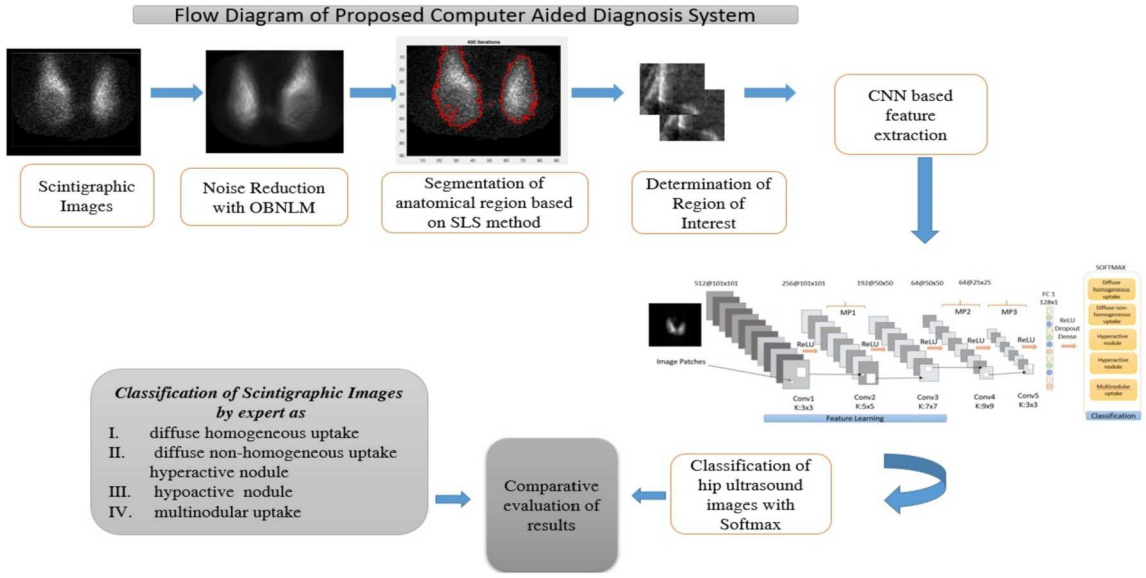

Figure **1.1: Flow diagram of proposed CAD system**

via shifting rectangles and by this way decreases the sensitivity of the image information to the shifts. There are increasing number of image classification (Arevalo et al., 2016; Wu et al., 2014) and segmentation (Yu et al., 2016; Chen et al., 2015) studies in the literature using CNNs, as well as the number of studies in the medical field based on CNNs. However the main obstacle in the medical field seems to be obtaining a high quality and adequate number of training datasets. To overcome this problem many data augmentation methods were employed in the literature like mirroring, rotation and scaling, all of which are suitable to rotation invariant datasets (Margeta et al., 2015; Tajbakhsh et al., 2015). In the lack of an adequate dataset another approach is to use transfer learning based CNN which is not suitable to our study because of the unavailability of present pre-trained CNN's resembling our dataset (Shin et al., 2016; Ma et al., 2017). Therefore we proposed to augment our dataset with rotation and scaling.

After determination of the ROI and augmentation of the dataset, different CNN architectures were constructed with different number of layers and size of convolutional kernels in each layer. The effect of different size and quality of datasets were also measured in each CNN configuration. By this way we determined the best configuration of the CNN to be employed in classification of thyroid nodules. The flowchart of proposed CAD system is presented in Figure 1.1. In summary we highlight the main contributions of this work as follows :

— Classification of the thyroid nodules were achieved with the custom made CNN architecture which extracts shape and texture features to recognize thyroid types from automatically determined ROI. The results of proposed CAD system were compared with the classification result of the expert. We proposed a promising CAD system which produced very similar result with an experienced doctor.

— This study is unique in the literature in the way of automatically classification of subclass of thyroid nodules.

2 LITERATURE REVIEW

Thyroid nodules are one of most commonly nodular lesion in the adult population. Most thyroid nodules are benign and only 7% turn out to be malignant. However, 15% - 30% of thyroid 10 nodules are diagnosed as indeterminate or suspicious for malignancy (Vorländer et al., 2010). The incidence of thyroid cancer has been reported to increase 2.4-fold over the last 30 years (Zhu et al., 2009). This increase is among the largest increases that has happened in all types of cancers.

Diagnosis of thyroid nodules depends on careful clinical examination and a series of imaging modalities. Thyroid ultrasonography (TUS) and thyroid scintigraphy are commonly used imaging modalities due to their noninvasive nature. Ultrasonography is useful in terms of defining the volume and localization of nodules. It is used as a guide to fine needle aspiration biopsy. Thyroid scintigraphy is a modality of nuclear medicine by which the functionality of thyroid tissue and nodules can be detected. Thyroid scintigraphy can sort the thyroid nodules according to their uptake as hypo or hyperactive. Besides its local diagnostic utilization scintigraphy is also useful in detecting distant metastasis of thyroid malignancy.

Common properties of ultrasound and scintigraphy images are speckle noise, intensity inhomogeneity of tissue texture and low contrast which render segmentation of thyroid nodules and computer aided detection (CAD) a challenging task. Ultrasound has been employed extensively to discriminate throid nodules. In the ultrasound studies Active Contour methods were employed to utilise intensity features to guide contour evolution. The accuracy of contour directly affects estimation of shape, size, and position of thyroid nodule and the classification success. Increasing accuracy decreases the number of false positives and improves the diagnosis of thyroid nodules.

An accurate contour estimation plays a significant role in classification and estimation of shape, size, and position of thyroid nodule. This helps to reduce the number of false positives, improves the accurate detection and efficient diagnosis of thyroid nodules. Koundal et. al. introduced an automated delineation method named as Spatial Neutrosophic Distance Regularized Level Set (SNDRLS) based on Neutrosophic L-Means (NLM) clustering which incorporated spatial information for Level Set evolution. Their method integrated spatial information with neutrosophic clustering and level-sets for accurate and effective segmentation of thyroid nodules in ultrasound

images (Koundal et al., 2016).

Variable Background Active Contour (VBAC) was proposed for nodule detection in ultrasound images (Savelonas et al., 2009; Maroulis et al., 2007). The VBAC model does not require pre-processing. It accurately detects more than one nodule simultaneously and offers topological variations and edge independency compared to ACWE method. ACWE is an initial contour dependent method. Tsantis et al. proposed the integration of Hough transform and wavelet-based edge detection method, namely hybrid multi-scale model (HMM) for the segmentation of nodules in ultrasound images (Tsantis et al., 2006). HMM requires a priori estimation of the shape of the nodule boundaries, as a drawback. Therefore, it was not able to detect elliptical benign nodules and malignant nodules with irregular boundaries. To overcome the drawback of VBAC, Iakovidis et al. Proposed automatic tuning of parameters by integrating the Genetic Algorithm (GA) with VBAC known as GA–VBAC model for nodule segmentation in ultrasound images with (Iakovidis et al., 2007).

Thyroid boundary detector was presented for the detection of borders of thyroid gland tissue. It utilized the knowledge of initial ROI pre-produced with feature extraction and classification methods in ultrasound images (Keramidas et al., 2007). The joint echogenicity-texture model (JET) evaluated the intensity of image and linear binary pattern (LBP) distributions by Mumford–Shah function at the same time to deliniate thyroid nodules (Savelonas et al., 2009). The JET model incorporated the advantages of VBAC to dicriminate hypo-echoic ,hyper-echoic and iso-echoic nodules and disangaged the topological adaptability drawback of HMM. The drawback of the JET model was its low power to distinguish structures such as bigger blood vessels from actual nodules. Thyroid nodule detector (TND) system was introduced for segmentation of thyroid nodules in ultrasound images and videos with more than 95% accuracy (Keramidas et al., 2012). Ma et al. proposed a method based on edge information of active contour model for contrast enhancement, smoothing and segmentation . Nevertheless, this method was dependent on human intervention for the determination of initial contour (Ma et al., 2010).

Ding et al. (Ding et al., 2011) utilized thyroid elastograms to extract statistical and textural features to train SVM for malignancy detection in thyroid nodules with a 95.2% maximum classification accuracy. Singh et al. (Singh and Jindal, 2012) achieved a maximum classification accuracy of 84.62% in classification of thyroid nodules by

extracting 13 gray level co-occurrence matrix (GLCM) features to train SVM. Acharya et al.(Acharya et al., 2012)(Acharya et al., 2012) also used SVM to classify thyroid nodules after extracting fractal dimension, local binary pattern, laws tex ture energy features. Although those handcrafted methods presented encouraging results, they required a series of pre-processing in the form of extraction of effective features. In fact, the difficulty in the pre-processing step is the selection of the most significant feature.

Jinlian et al. proposed a hybrid method for thyroid nodule diagnosis, which was a fusion of two pre-trained convolutional neural networks (CNNs) with different convolutional layers and fully-connected layers. After separately pre-training the two networks with ImageNet database, they fused feature maps learned by trained convolutional filters, pooling and normalization operations of the two CNNs. A softmax classifier was used to diagnose thyroid nodules, with the fused feature maps. The proposed method was validated on 15,000 ultrasound images and the fusion of the two CNN based models lead to significant performance improvement, with an accuracy of 83.02% (Ma et al., 2017).

3 THYROID ABNORMALITY AND DATA ACQUISITION

3.1 Thyroid Nodules

Thyroid gland which is located anteriorly in the neck region of the human body is one of the major hormone secreting glands of the mammalian endocrine system. The thyroid gland consist of follicular cells that produce and store thyroid hormones within the thyroglobulin molecule. The thyroid gland depends on the presence of iodine and tyrosine to achive its function. The thyroid hormones plays a key role in the regulation of human metabolism and can affect almost every cell in the body. Insufficiency or over production of thyroid hormanes lead to pathologies in the gland and results in conditions which affect the whole body. Laboratory tests are important in diagnosing conditions of the thyroid gland. For the diagnosis of thyroid diseases clinical manifestations, blood hormone levels are used in combination with imaging modalities (Kirsten, 2000). The pathological conditions of the thyroid gland has a high prevelance in the population. The incidence of thyroid nodules increase by age. Nearly half of the population is affected by thyroid nodules until the geriatric ages. Scintigraphy of the thyroid is the sole modality for evaluation of the functional characteristics of thyroid gland and its pathologies (Hegedüs, 2004).

3.2 Scintigraphic Images

Scintigraphy is a modality used to determine the functional status of many organs. As a modality of nuclear medicine scintigraphical examination requires nuclear isotopes which are directed to the target tissue by human metabolism. The dependencty of thyroid gland to the Iodine for functioning renders the thyroid gland the target tissue of the consumed iodine molecule in the body. 99mTcO4- and 123I molecules are the two mostly used isotopes which are used for thyroid scintigraphy. These molecules are concentrated in the thyroid gland after their introduction to the human body and the level of radioactivity is measured by the scintigrahy machine which also produces medical images expressing the characteristics of the underlying conditions in the thyroid gland (Moreno-Reyes et al., 2016). The indications of thyroid scintigraphy in the clinical settings were summerised in the revised consensus statement of American Collage of Radiology, released in 2014. In this clinical guideline the thyroid scintigraphy was

stated to be useful in determining the size and location of thyroid tissue, in overt and subclinical hyperthyroidism and detecting suspected focal masses or diffuse thyroid disease. It was also advised to be used as a clinical laboratory test to detect the function of thyroid nodules. The thyroid scintigraphy can be used in differentiating hyperthyroidism from other forms of thyrotoxicosis (Spratt et al., 2016). The knowledge of the functional status of the thyroid gland can be used in the diagnosis of many benign throid diseases. In the case of thyotoxicosis ; a thyroid uptake of low levels is suggestive of subacute thyroiditis, on the other hand a normal or elevated uptake is consistent with toxic nodular goiter and Graves' disease. In the presence of increased uptake the shape characteristics of the distribution of the nucleotide were used to differentiate between nodular goiter(heterogenous) and Graves' disease(diffuse and homogenous) (Sarkar, 2006). The whole body thyroid scintigraphy is useful in determination of presence and location of ectopic thyoid gland or residual functioning thyroid tissue or cancer tissue after surgery or meatastasis (Spratt et al., 2016). According to Salvatori et al. most of the time(93.1%), there is a remnant throid tissue after total thyroidectomy operation and accurate estimation of remnant mass tissue is not possible by surgical report or ultrasonography in a considerable number of postoperative patients. According to the study of Ozdemir et al. on postoperative patients with differentiated thyroid carcinoma scintigraphy is the most sensitive method for diagnosis of the remant tissue unless the remnant tissue was successfully ablated by radionucleotide therapy (Ozdemir et al., 2016; D'Andrea et al., 2009; Salvatori et al., 2007). Therefore thyroid scintigraphy can be used to evaluate the status of functioning thyroid tissue both in the diagnosis stage and as a means of after-treatment control (Spratt et al., 2016).

3.3 Abridged Classification of Thyroid Diseases

Thyroid nodules are scintigraphically classified according to their ability to uptake the given isotope compared to that of the extranodular thyroid tissue. A cold nodule (hypofunctional) has a reduced isotope uptake and a hot nodule (hyperfunctional) has increased isotope uptake compared to the other parts of the thyroid tissue (Corvilain et al., 1998). Thyroid scan gives valuable information about the thyroid gland in the presence of thyroid abnormality in the thyroid scan (Hegedüs, 2004). Ultrasound guided fine-needle aspiration biopsy (FNAB) of the thyroid nodules is used widely to rule out the malignancy. The scintigraphic characteristics of the nodules may be used as a means of assistance before FNAB because nodules with increased uptake(hot nodules) are gene-

rally benign and do not require FNAB, while less functioning nodules (cold nodules) may be malignant) (Sarkar, 2006; Hegedüs, 2004). Thyroid scintigraphy is now mostly used in the work-up of a hyperfunctioning thyroid nodule. However the diagnosis of thyroid nodules of a patient with normal TSH values can be delayed unless thyroid scintigraphy is done. Hegedüs et al. stated that the risk of malignant thyroid nodules in the presence of normal TSH values to be higher than previously stated (Hegedüs, 2004). Although other clinical or radiographic measures like history, physical examination, laboratory tests, ultrasonography besides the scintigraphy may be needed in order to properly evaluate pathological conditions of thyroid gland, thyroid scintigraphy is still an important element for the diagnosis and clinical decision making of thyroid pathologies. There are scarce computer aided diagnosis studies which evaluate scintigraphic images of the human body. There are even fewer studies in the literature on thyroid scintigraphy image.

In this study common pathological patterns of scinticraphic images of thyroid gland were classified by the proposed CNN. These patterns include thyroid glands with diffuse homogenous uptake, diffuse nonhomogenous uptake, solitary nodules with either increased or decreased uptake levels and multinodullary thyroid glands. According to these scintigraphic images there were 5 groups of scinticraphical appearance. The images with normal thyroid uptake and postoperative patients having no uptake were excluded from the study.

3.3.1 Diffuse homogenous uptake

This group includes scintigraphic images of thyroid glands with even distribution of increased isotope uptake in the gland (Fig. 3.1). In a thyrotoxic patient this appearance is reported as Grave's disease. In this condition the gland is usually enlarged to some degree.

3.3.2 Diffuse nonhomogenous uptake

This group also includes images of enlarged thyroid glands with increased homogenous uptake in the glandular tissue but having distortions from the normal glandular shape, probably due to congenital or developmental conditions leading to anatomical distortions in the gland, periglandular pathologies or nonfunctioning regions of the glandular

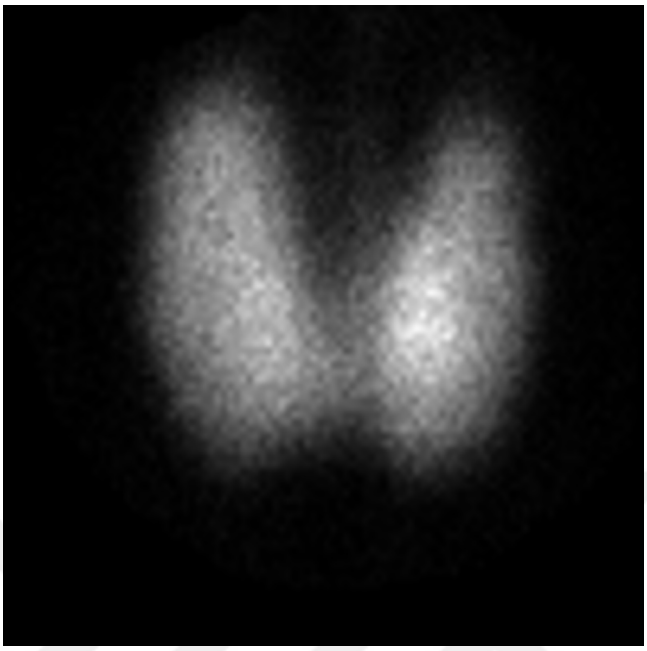

Figure **3.1: Demonstration of scintigraphic diffuse homogenous uptake image**

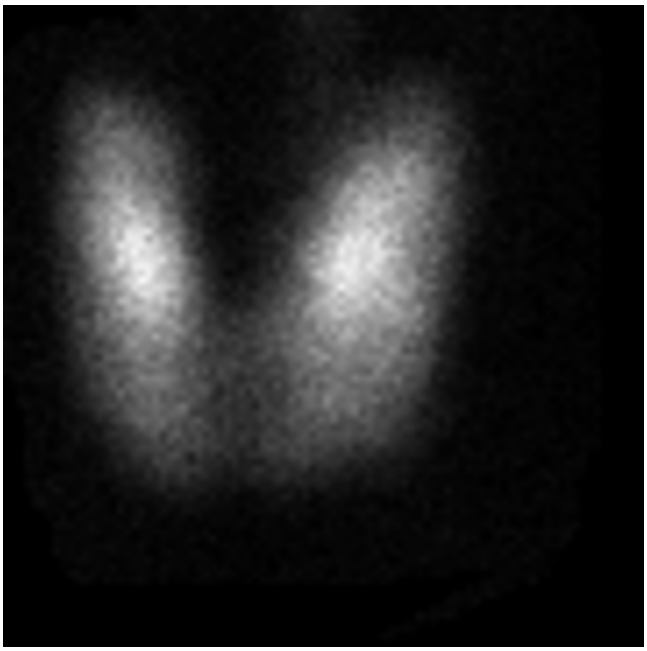

Figure **3.2: Demonstration of scintigraphic diffuse nonhomogenous uptake image**

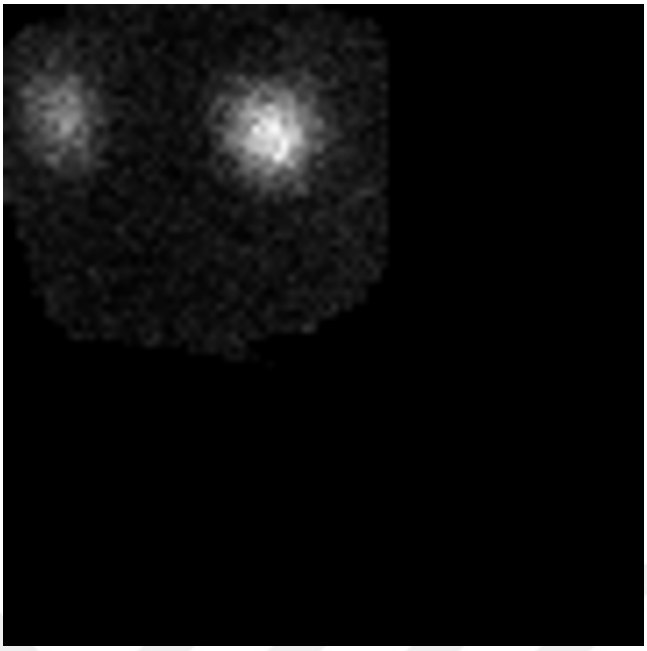

Figure **3.3: Demonstration of scintigraphic hyperactive nodule image**

tissue itself (Fig.3.2).

3.3.3 Hyperactive nodule

Group 3 (Hyperactive nodule) : This group constitutes thyroid images with local increased uptake in the glandular tissue. The accumulation of isotope in the gland is mostly round in shape and usually does not cause so much distortion in the global structure of the gland (Fig. 3.3).

3.3.4 Hypoactive nodule

Thyroid gland images including a clearly visible solitary area of low accumulation of isotope in the glandular tissue were labelled as group 4. The general characteristics of images of lesions in these thyroid glands resemble group 3 although these lesions does not accumulate the given isotope (Fig. 3.4).

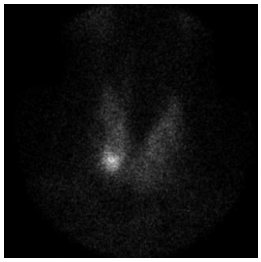

Figure **3.4: Demonstration of scintigraphic hypoaactive nodule image**

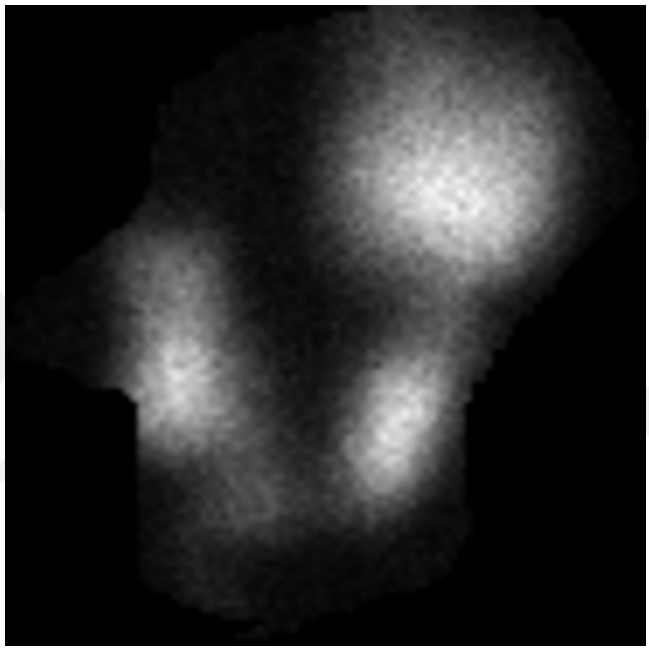

Figure **3.5: Demonstration of scintigraphic multinodular uptake image**

3.3.5 Multinodular uptake

This group contains images of enlarged thyroid glands with heterogenous uptake due to multiple nodules which has differing degrees of isotope accumulation capacity (Fig. 3.5). Generally the outer borders of the gland is also distorted. Patients with toxic multinodular goiter were included in this group.

We have collected 954 scintigraphic images from Sisli Etfal Training and Research hospital. Our data set consist of 372 diffuse homogeneous uptake, 152 diffuse non-homogeneous uptake, 185 hyperactive nodule, 41 hypoactive nodule and 204 multinodular uptake images.

4 IMAGE PRE-PROCESSING OPERATIONS

Image pre-processing steps are very important in the recognition of pathologies. When we use whole image in a CAD system, it will try to extract meaningful information on the other anatomical regions. Instead of feeding deep neural network architecture with whole image, we try to give only images which has a only region of interest. For this reason we have segmented thyroid nodules from scintigraphic images.

Region based active contours methods are very succesfull methods in order to segment region of interest. With the Chan-Vese method (Wang et al., 2010), we initialize a initial contours on the image. By optimizing the force applied to this contours, we can determine the different regions in the image. However, Chan-Vese method known as a robust method for image noise, the segmentation success is under desired level. Because this method is highly depend on the location of initial contours. It can not handle successfully image intensity non homogeneity problem.

Statistical level set model(Zhang et al., 2010) handles the weak points of Chan-Vese model by transforming image into other domain, by this way it can define different inhomogeneous objects in the image with Gaussian distribution of different means and variances.

After determination of region of interest, we need to further image pre-processing operation. Statistical level set method is robust to the speckle noise but when we decrease noise, the intensity inhomogeneity problem is also decreased. Noise reduction provide to improve image segmentation success.

CNN try to extract meaningful information from images. We assume to improve success of CNN by elimination of unnecessary anatomical regions and decrease the irrelevant information comes from the speckle noise. For this reason we removed speckle noise present in images by OBNLM method (Coupé et al., 2009).

The accuracy rate of CNN is highly depended on the number of data used in the training dataset. In the literature different types of data augmentation is present as rotation, scaling, translation and mirroring. In this study we try to increase number of dataset by noise reduced images. For this reason we have combined original dataset

with the noise reduced images based on the OBNLM method.

4.1 Active Contours Model

Image segmentation is the process of sectionalizing an image into homogeneous parts in terms of color, texture, intensity or another common property. There are many methods proposed to segment images of which the active contours models are the most practiced and reliable methods in the literature. The main idea of the active contours models are defining the borders of a region based on an energy minimizing policy. Active contours models direct curves by optimizing the interior and exterior force applied to the initial contour resulting with a series of shrinking and expanding operations to define the true border of the region (Chan and Vese, 2001).

The active contours models are categorized into three groups as edge based, region based and hybrid models. Edge based models use image gradient information to localize a region (Paragios and Deriche, 2000). In the presence of noise and weak boundaries the edge based methods exert low performance. Region based active contours models are not dependent on the image gradient. These models use statistical information of an image to evolve the curves which helps to sort through the region of interest despite of weak and deficient edges. CV method is one of the most popular example of the region based models (Chan and Vese, 2001).

4.2 Chan-Vese Model

The Chan-Vese model can be accepted as a simplified variant of Mumford –Shah (MS) function into a level set framework to represent an image as a piecewise constant function. MS model utilizes a set of contours C to distinguish different homogenous regions of interest in an image. CV successfully works out the optimization problem by defining unknown curve C with level set function. CV model is reformulated with level set function $\phi(x)$ to find out optimum contour C which distinguishes homogeneous

image into non overlapping regions as follows :

$$E^{CV}(c_1, c_2, C) = \mu \cdot \text{Length}(C)$$

$$+ \lambda_1 \int_{\omega} |u_0(x,y) - c_1|^2 H(\phi(x,y))\mathrm{d}x\mathrm{d}y \tag{4.1}$$

$$+ \lambda_2 \int_{\Omega\backslash\varpi} |u_0(x,y) - c_2|^2 (1 - H(\phi(x,y)))\mathrm{d}x\mathrm{d}y$$

An evolving curve $C = \partial\Omega$, with $\omega \subset \Omega$ an open subset, inside the contour was demonstrated with the parameter ω and outside the contour with the parameter $\Omega\backslash\varpi$ which represents the background pixels, $H(x)$ represents the Heaviside function. c_1 and c_2 are the values of u_0 which are the average intensity values inside and outside of the contours C. λ_1 and λ_2 parameters are very important to control the force applied to inside and outside the contour. It may be better to determine small values of μ when we try to segment small size of objects. In this study, we take λ_1 value smaller than λ_2 value. The energy function was minimized with the level set formulation Eq. (4.2).

$$C = \partial\omega = \{(x,y) \in \Omega : \phi(x \cdot y) = 0\}$$

$$\omega = \{(x,y) \in \Omega : \phi(x \cdot y) > 0\} \tag{4.2}$$

$$\Omega\backslash\varpi = \{(x,y) \in \Omega : \phi(x \cdot y) < 0\}$$

The main merit of the CV model being not depend on the image gradient is a powerful property for segmentation of blurred and deficient objects in a noisy image. Although CV constitutes the theoretical background of many segmentation methods the usage of constant parameters as the global information of the image causes inadequate segmentation results of CV model in inhomogeneous images. Moreover success of the energy function is dependent on the initial contour position.

4.3 Statistical level set model

Statistical level set model emerged so as to overcome the segmentation difficulty of inhomogeneous images for which the piecewise constant function of the CV model is not convenient. The statistical level set model defines objects by means of multiple Gaussian probability distributions of spatially varying means and variances which is useful in conditions where the image contain inhomogeneous target objects (Zhang et al., 2010).

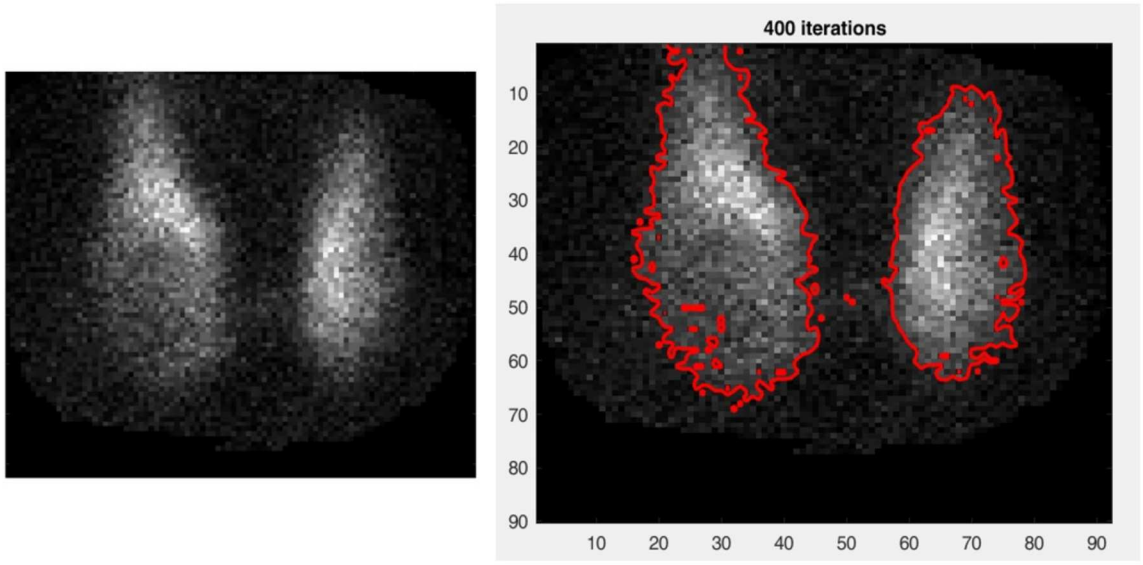

Figure **4.1: Demonstrate segmentation original scintigraphic images and its segmentation result based on statistical level set method**

Probability density function $P(I(y)|\theta_i, B, x)$ utilises the different mean parameter $U_i(x)$ to define varying local region statistics in Eq. (4.3). This model assumes that there exist n objects in the image domain Ω, where Ω_i represents i^{th} object domain. The parameter x stands for the center pixel of each local region O_x.

$$P(I(y)|\theta_i, B, x) = \frac{1}{\sqrt{2\pi\sigma_i}} \exp\left(-\frac{(I(y) - U_i(x)^2}{2{\sigma_i}^2}\right) \tag{4.3}$$

For a successful discrimination of all object regions in original image intensity domain $D(\tau)$ adjacent regions should have non-overlapping properties in the statistics. This issue can be handled by mapping the image to another domain $R(\tau)$ by averaging image intensities within the predefined window size. The following energy function was minimized with the regularized level set function Φ.

$$E^L_{\theta,\beta,\Phi} = \sum_{i=1}^{N} \int_{\Omega} F_i(y) M_i\left(\Phi(y)\right) \mathrm{d}y \tag{4.4}$$

The statistical level set model is a soft classification method which assigns each pixel to more than one class. In this method each inhomogeneous objects are identified with Gaussian distribution of different means and variances. The intensity in the transformed domain is calculated by averaging the adjacent pixel intensities of the same class. Classification result is less sensitive to noise because the intensities in the transformed domain have less overlapping in the statistics than those in the original domain. This

method even can be used for bias correction because it acts as a means low pass filter by averaging the adjacent pixel intensities of the same class in the transformed domain (Zhang et al., 2010). This method however is dependent on the initial contour. In this study all scintigraphic images were segmented with statistical level set method (Fig. 4.1).

4.4 Noise Reduction with Optimized Bayesian Non-Local Mean

Successful image denoising the anatomical landmarks in the ROI become more prominent and clear which increases visual perception. This fact led us to hypothesize that image denoising procedure to improve the success of the proposed CNN based CAD system. Because the false signals coming from image noise are preserved by the CNN and this information is processed by the system as if it is meaningful. The reduction of these non-significant information in the training dataset might have a positive effect on the training phase.

The noise reduction in medical images is not an easy problem since the speckle artefacts are hard to model and the speckle noise is tissue specific. It is crucial to preserve the critical anatomical information during noise reduction in the ultrasound images. Non local mean (NLM) filter is a widely used and successful image denoising method. NLM method divides the image into several overlapping blocks. The NLM calculates the similarity of the reference block (the search window) with the remaining blocks of the image represented by its mean weight value. By this way NLM can accomplish noise reduction not only in the close proximity of the selected block but also in the blocks of a distance, that is the whole image. However NLM filter was originally developed for additive Gaussian noise not for speckle noise of ultrasound images. Pierrick et al. remodeled the non-local mean filter called as OBNLM by occupying Loupas noise model which is one of the most successful speckle noise models in the literature (Coupé et al., 2009) . The distance measurement metric in OBNLM was also changed with Pearson distance measurement metric because L2 similarity metric may work inaccurately in low signal to noise ratio images like scintigraphic images. OBNLM outperforms other well known methods in the literature like local adaptive filter and anisotropic diffusion filter (Zhang et al., 2015).

In this study we applied OBNLM method to scintigraphic images with the smoothing

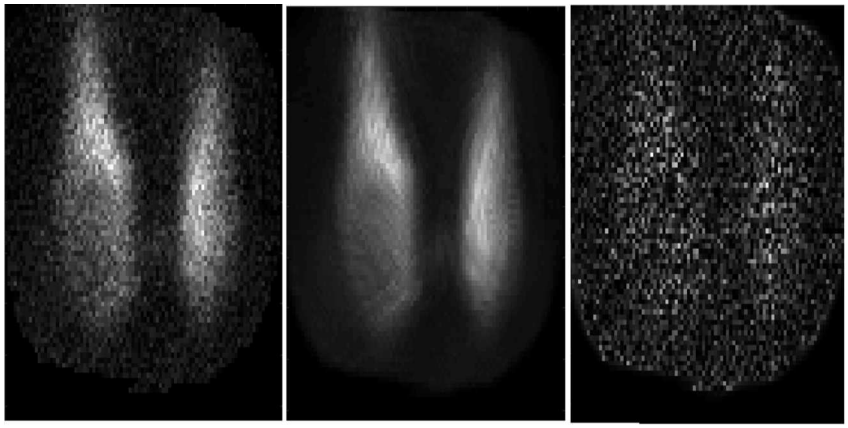

Figure **4.2: Demonstration of a) scintigraphic image of thyroid nodule, b) denoised scintigraphic image by OBNLM method with smoothing parameter (h=5) and search area size (W=7) and, c) corresponding residual image**

parameter (h=5) and search area size (W=7) to provide a more clear and augmented training dataset. Each center pixels x_{ik} of blocks B_{ik} were empirically estimated with the parameter $\widehat{v}(B_{ik})$ based on equations Eq. (4.5) and denoised scintigraphic images were obtained as demonstrated in Figure 4.2.

$$\widehat{v}(B_{ik}) = \frac{\frac{1}{\Delta i_k}\sum_{j=1}^{|\Delta_{ik}|} v(B_j)p(u(B_{ik})|v(B_j))}{\frac{1}{\Delta i_k}\sum_{j=1}^{|\Delta_{ik}|} p(u(B_{ik})|v(B_j))} \tag{4.5}$$

4.5 Principles of The Proposed Image Pre-processing Steps

The thyroid nodules has complex anatomical and histological structure resulting in both global and local intensity inhomogeneities. Thus a proposed system must handle both global and local inhomogeneity problem in such a complicated anatomical area. The statistical level set method which was stated to be more precise than other methods in segmentation of inhomogeneous objects even in the presence of high noise was selected for segmentation of thyroid scintigraphic images (Zhang, Zhang, Lam and Zhang, 2016).

The CV model and SLS methods were applied to the original image to segment necessary anatomical area. The SLS method was more successful in segmenting anatomical areas than the CV model. Speckle noise were reduced by OBNLM method in order to obtain noise free training and test data set. By this way we assumed to increase accuracy of our proposed CNN architectures.

5 CONVOLUTIONAL NEURAL NETWORK

5.1 Layers used to build Convolutional Neural Network

Deep CNNs, being one of the advanced visual analysis methods, are the hot topic of the literature. CNNs are synergetic multilayered mechanisms which are mainly composed of convolution layer, activation function and pooling layer. These layers work in a cascaded and hierarchic manner. The output of one layer is served as an input to the following layer. The architecture of a CNN can be manipulated according to the specific pattern recognition problem. There may be various intermediate layers to extract effective low level features which are used to build high level features. The learning capability of CNNs is a result of their analytic capacity of the hierarchy of these effective features.Resembling mammalian visual neurons, every neuron of a layer is connected to its own specific region of image which commonly overlap to other neuronal output. The texture and geometrical structure of an image may be represented by CNNs by analyzing the overlapping information of local areas defined by each neuron.

Representation of images with increasing comlexity may require manipulation of the depth and breadth of a network. Estimation of optimum depth and breadth of a CNN configuration designed for a specific goal has no strict rule proven mathematically. The pathway of CNN architecture optimization is an expert dependent approach which is principally a trial and error minimization approach. Likewise, training is through minimizing a loss function which produces information to feedback the CNN. A typical CNN has the ability to recognize texture and shape characteristics of an image by utilizing perceived information of each neuron. These neuronal information is the raw data which convalesce after processing it through cascaded learnable filters and subsampling operations.

5.1.1 Convolutional Layer

The key element of the CNN is the convolutional layer. It has a particular importance in extracting features from the raw image. It uses learnable filters each of which represents a specific portion of the image called as a local receptive field. Every kernel is slidable on the image, the magnitude of which is defined by the stride parameter. A feature map is produced by the convolving operation according to the width and height of the input

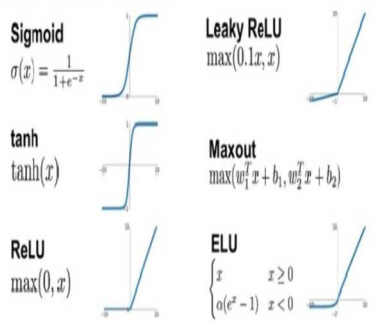

Figure **5.1: Demonstration of different activation function**

volume. Convolution layer is very important to obtain feature maps. The size of kernel and stride parameters used in this layer is very important to extract texture features. We used cascaded convolution layers and try to avoid using max pooling operations to not loose important features.

5.1.2 Activation function

Activation function uses the feature maps produced by the convolutional layer as input information. Features produced by different filters in the convolutional layer are learned by the activation function. Stacking of all of the activation maps results with the production of the full output volume. A non-linear problem requires an activation function which adds non-linearity to the system. Recently introduced the so called rectified linear unit (RELU) is the mostly utilized one. RELU avoid easy saturation of gradient descent algorithm. RELU replaces negative values of the feature maps with zero which considerably increases the speed of the convergence of the CNN. In this thesis we haven implemented RELU with using max function, it provide us to define negative values with zeros. Non linear activation function of RELU allowed the nodes to learn more complex shape and texture information in the images. The result is better than the other activation function of sigmoid and Tanh activation function (Fig.5.1).

5.1.3 Pooling Layer

The pooling layer is a form of down-sampling which provides to reduce feature maps. The max and average pooling are the mostly used non-linear functions by the pooling

layer. The main function of the pooling layer is to prevent over fitting by decreasing the amount of parameters and computation. The output of the convolution and pooling layers are high level features extracted from image. The fully connected layer of CNN utilizes these discriminative features as input and provides classification of the test data according to training dataset.

5.1.4 Fully Connected Layer

Every neuron at the previous layer is connected to every neuron at the next layer by using the fully connected layer. The main purpose of fully connected layer is to determine the class (or label) of the given test input image according to the train data by using the its high-level features. Another advantage of using fully-connected layer is getting better result by using the combination of two good features gathered from the previous layers.

5.2 Our Proposed CNN

CNNs are multi-layered structures. There are 4 types of layers which process the gathered information from the neurons namely; convolutional, activation, pooling and fully connected. Every layer performs a different task in the network. Similar to the working principle of a mammalian retinal neuron, each neuron receives a local area of the image producing an overlapping representation of it in the convolutional layer. The function of the convolutional layer is to create feature maps. These feature maps are produced depending on the weights of the neuronal inputs in which the shared weights constitute a filter for each map. The main function of them is to prevent over-fitting in other words to increase efficacy. The following layer is the activation layer after the convolutional layer. More complex features are extracted in the activation layer with the aid of nonlinear property of the activation layer. In the following pooling layer, inputs are statistically analyzed and the sensitivity of the image is decreased through shifting rectangles.

After determination of the ROI different CNN architectures were constructed with different number of layers and size of convolutional kernels in each layer. The effect of different size and quality of datasets were also measured in each CNN configuration. By this way we determined the best configuration of the CNN to be employed in

Table**5.1: Details of proposed CNN components (Conv : Convolutional Layer,MP : Max pooling layer, FC : Fully connected layer)**

Layer	Input size of the image	CNN (filter size and feature maps)	Stride
Conv1	101x101	9x9x256	1
Conv2	101x101	7x7x192	1
MP1	50x50	2x2	2
Conv3	50x50	5x5x512	1
MP2	25x25	2x2	2
Conv4	25x25	9x9x256	1
MP3	12x12	2x2	2
FC1	128		

classification of thyroid nodules.

The enormous capacity of CNNs to solve a specific problem can be tuned by modulating their architecture in order to increase the success of the system. By changing the hierarchical organization of the CNNs or the number of the layers the ability of the system can be modified in order to reach the desired goal. For example, shallow CNNs are used to recognize basic structures such as lines and edges. By increasing the depth of the CNNs more complex structures like shape and texture can be learned by the system (Ma et al., 2017; Zhang, Xiao, Dai, Suo, Wang, Shi and Zheng, 2016). In addition the number and size of filters used in convolutional layer or the magnitude of reduction in the pooling layer can be manipulated which provides a superb versatility to the system. However there is no theory proof in order to construct the most suitable CNN to achieve a desired goal (Ghesu et al., 2016). Basically it is a trial and error approach which minimizes the error of the system.

In order to construct a successful CNN structure one should be familiar to the anatomical relationships and pathophysiological conditions to be recognized by the system. In the scintigraphic images shape and texture characteristics of thyroid nodules are the prerequisites for the explanation of the condition. The anatomical structures of nodules may show variations in each person. Moreover each scintigraphic image exerts a slightly different relationship between anatomical structures causing changes in the shape information. In our CNN configuration in order to preserve low level texture and shape features from the aggressive reduction operation of pooling layer, we employed three convolutional layers successively without a pooling operation in between. The neuronal information captured from the image called as the receptive field, should be smaller than the structures to be recognized to avoid irrelevant and nonlocal informa-

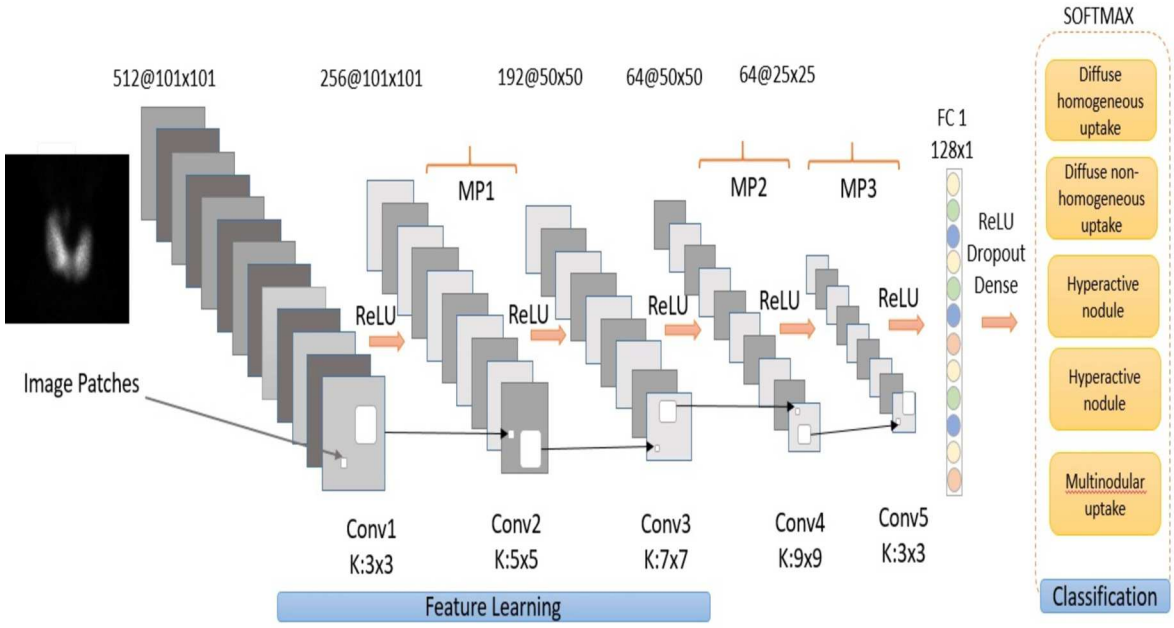

Figure **5.2: Architecture of our proposed CNN**

tion (Anthimopoulos et al., 2016). In our problem the anatomical structures which are in different size and shape should be recognized from the each image. Therefore different size and number of filters were used in each convolutional layer with respect to size of the target objects. We employed different filter sizes of 3-5-7-9 in each convolutional layer demonstrated in Table 2.

The proposed CNN consists of four convolutional and three max pooling layers in the feature learning step. Image patches sized 101x101 were given to the first convolutional layer and 256 feature maps of size 101x101 were generated. In each step, we have determined number of feature maps in each step by trying different number of feature maps. We utilized cascaded convolution layer. In the second convolution layer, we have created 192 features maps with filter size of 7x7. Next to the second convolutional layer we placed a rectified linear unit (ReLu) which replaces negative value of feature map with zero. The third convolutional layer which has the kernel size of 5x5 was placed and 512 feature maps of size 50x50 were generated. Pooling operation was employed after the convolution and activation function (ReLu). Max-pooling was applied to feature maps with the stride size of two pixels. The fourth convolutional layer generated 256 feature maps of size 25x25. Fully connected layer with 128 hidden units with max-out activation function was stacked to label each image patches. Max-out activation function is known also as softmax function, softargmax or normalized exponential function.

For the optimization algorithm, we used Adam algorithm instead of classical stochastic gradient descent to update network weights in the training data. Its name was derived from the first two letters of the words adaptive and moment. Adam is an adaptive learning rate method, in other means, it puts into account individual learning rates of many parameters. Basically, it uses estimations of first order (mean) and second order (uncentered variance) moments of gradient, separately, to calculate the learning rate of individual weights of CNN. In addition, the gradient of the cost function of neural network may be regarded as a random variable, because of the partial evaluation of a piece of randomly selected batch of data. During estimation of the moments. Adam algorithm evaluates exponentially moving averages which are calculated utilizing the gradient values of a mini-batch. Adam algorithm combines advantages of the Adaptive Gradient Algorithm (AdaGrad) and Root Mean Square Propagation (RMSProp). For this reason Adam algorithm works fast and better than AdaGrad and RMSProp.

we have divided our dataset into training and test set. Our proposed model used to training dataset to learn more robust feature and test set were utilized to classify scintigraphic images with trained weights. We aimed to obtain the probability of each groups from softmax function of the classification step of our proposed CNN as diffuse homogeneous uptake, diffuse non-homogeneous uptake, hyperactive nodule, hypoactive nodule and multinodular uptake images.

6 COMPARATIVE MODELS

The performance of the proposed CNN based CAD system was compared with state of art methods like pyramid of histograms of orientation gradients (PHOG)(Bosch et al., 2007), gray level co-occurrence matrix, local configuration pattern and bag of feature (BoF)(Deselaers et al., 2008).

6.1 Pyramid of Histograms of Orientation Gradients

PHOG is the extended version of the HOG method which was designed to extract shape feature from images. PHOG is capable of determining the local shape of the object based on distribution over the edge orientations and spatial layout by decomposing the image into subbands at multiple resolutions (Bosch et al., 2007). PHOG was used for recognition of emotional status of human face (Dhall et al., 2011) and other human face expressions in the literature such as smiling (Bai et al., 2009), fatigue (Zhao et al., 2013) and recognition of vehicles for traffic surveillance (Ghasemi and Safabakhsh, 2012).

PHOG descriptor provides to represent the local shape of an object by using histogram of edge orientation in a specific region divided into subbands expressed in the fractions of K bins. The histogram of edge orientation is estimated based on image edge gradient and magnitude. The decomposition of the image into subbands in x and y dimensions creates cells. It is designed as a multilevel method with increasing number of subbands at each pyramid level. PHOG provides to calculate HOG features in each subbands thus generating finer shape features at increasing levels. In this study we extracted edge information from image patches of thyroid nodules by using Canny Edge detector. Afterwards the image was partitioned into cells at three pyramid levels. Each level L contains 2L cells in the grid. The 3x3 Sobel mask was operated on the edge contours of each cells to obtain orientation gradient without any smoothing operation (Fig. 6.1). The magnitude of the edges determine their contribution and the assigned weights. The frequency within a certain angular range and orientation is simulated as a bin in the histogram (Fig. 6.2). The results of HOG method were concatenated to obtain the K bins histogram of PHOG. The resulting histogram is the sum of information obtained from each level of pyramid representation. In our experiment parameters of the HOG descriptor were determined as 8 and 20 orientation bins in the ranges of [0-180] and

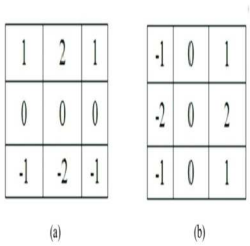

Figure **6.1: Shows sobel masks for gradient a) horizontal and b) vertical components**

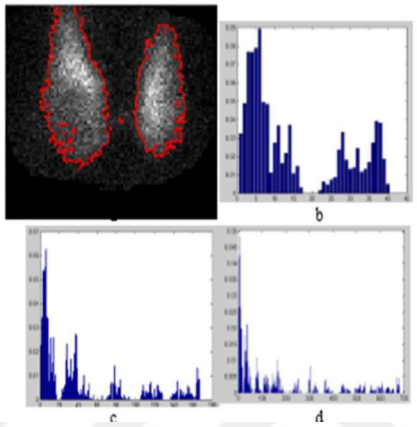

Figure **6.2: Demonstrate frequency within a certain angular range and orientation**

[0-360]. The best results were obtained assuming the number of pyramids L=3 and bin size K=8 and orientation range is [0-360]. The number of features extracted based on PHOG method from scintigraphic images can be determined as follows K represent bins of histogram and L is the number of level in image pyramid representation. We have extracted 168 shape features for L=3, K=8 and range R =[0=360].

6.2 Gray Level Co-occurrence Matrix

GLCM, is one of the well-known and widely used texture analysis methods and also known as gray tone spatial dependency matrix. GLCM is a frequency matrix which calculates sum of repetition of pair of intensity values in an image in a given displacement (d :distance) and orientation (θ :angle) also named as offset. The GLCM matrix calculates the second order joint conditional probability density function (PDFs) of gray level pairs in an image. Varying offset values will give changing GLCM matrices and different co-occurrence distributions which will result in different image features for the same reference image (Fig. 6.1).

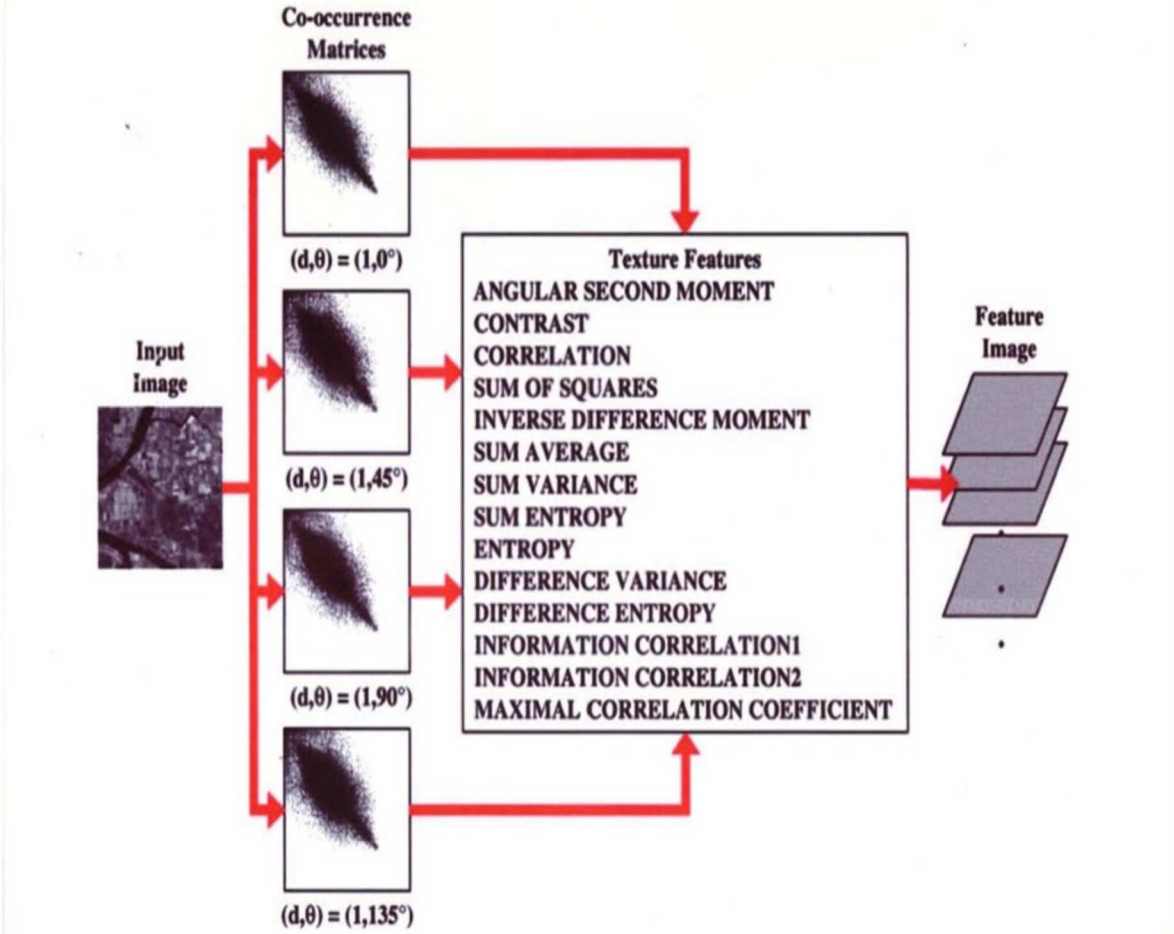

Figure **6.3: Shows of GLCM matrices and different co-occurrence distributions**

GLCM of an image is computed using displacement vector d (distance : distance to the adjacent neighbor) and rotational angles (preferably θ :0^0 ,45^0 ,90^0,135^0). An example is given in Fig. 6.2 a. In Fig. 6.2 b., image intensity values are given in the form of a matrix. Fig. 6.2 demonstrates calculated GLCM where (i, j) represents the number of times a point having gray level j occurs relative to a point having gray level i for offset d=1 and θ= 0 .

Widely used texture features that can be obtained from GLCM are contrast, energy, homogeneity, correlation and entropy. We calculated also other metrics derived from GLCM as angular second moment (ASM), variance, difference variance, difference entropy, difference moment and two measurements of correlation features .

Calculated features : Autocorrelation, Contrast, Correlation, Cluster Prominence, Cluster Shade, Dissimilarity, Energy, Entropy, Homogeneity, Maximum probability, Sum of squares, Sum average, Sum variance, Sum entropy, Difference variance, Difference entropy, Information measure of correlation1, Inverse difference normalized, Inverse difference moment normalized In this study we have computed all of the above second order features stated above for each of the symmetric and non-symmetric GLCM created at different displacement and orientations (θ : 0^0 ,45^0 ,90^0,135^0 Offset= 8,12,16). For each of the calculated GLCM different features were extracted and used for classification of images.

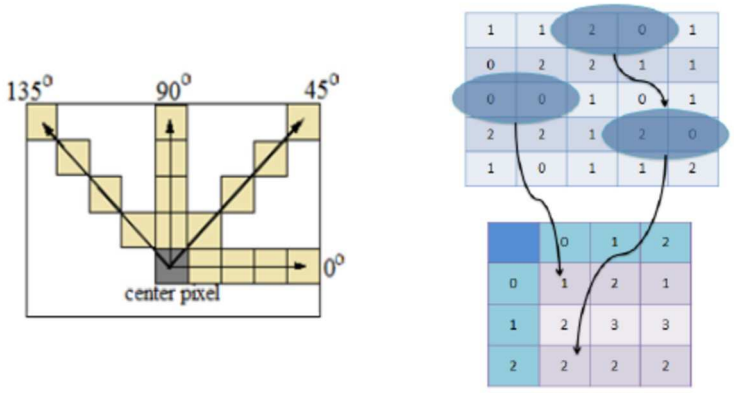

Figure **6.4: a)Demonstrate displacement vector of GLCM matrices and b) different co-occurrence distributions**

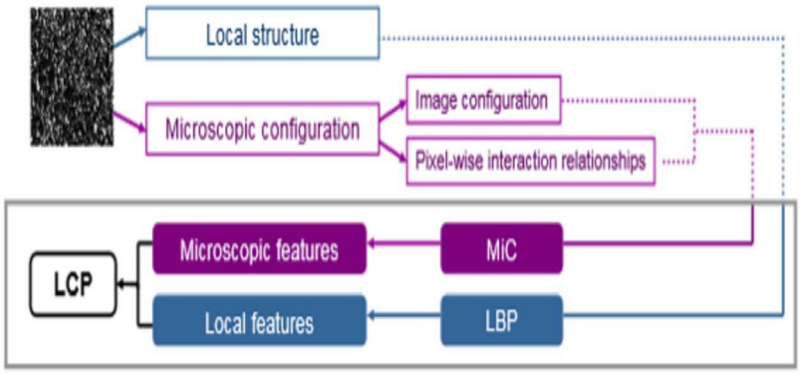

Figure **6.5: Diagram of local and microscopic features for local configuration pattern**

6.3 Local Configuration Pattern

Local configuration pattern can be obtained by combining microscopic images descriptor (MiC) with local features represented by pattern occurrences as demonstrated in Figure 6.3. The descriptor MiC that encodes image microscopic configuration by a linear configuration model.

For Local Binary Pattern : The binary value of "0" or "1"assigned to the neighboring pixel according to center pixel value. Value "0" is considered if the pixel value is greater than neighboring pixels, otherwise "1". A local contrast information is thus extracted from LBP. The segmented scintigraphic images in this work are divided into rows and columns where each individual grid is represented by the pixel value. After applying LBP, the image is represented by binary numbers (0s and 1s). Then, the frequency of the recurring number in each grid is computed and mapped to a histogram as shown i Figure 6.4.

For Mic Descriptor : Microscopic features capture image microscopic configuration which embodies image configuration and pixel-wise interaction relationships by a linear model. The optimal model parameters are estimated by an efficient least squares estimator. To achieve rotation invariance, which is a desired property for texture features, Fourier transform is applied to the estimated parameter vectors. Finally, the transformed vectors are concatenated with local pattern occurrences to construct LCPs. The Steps of algorithms

— Compute the LBP code image and apply mapping table

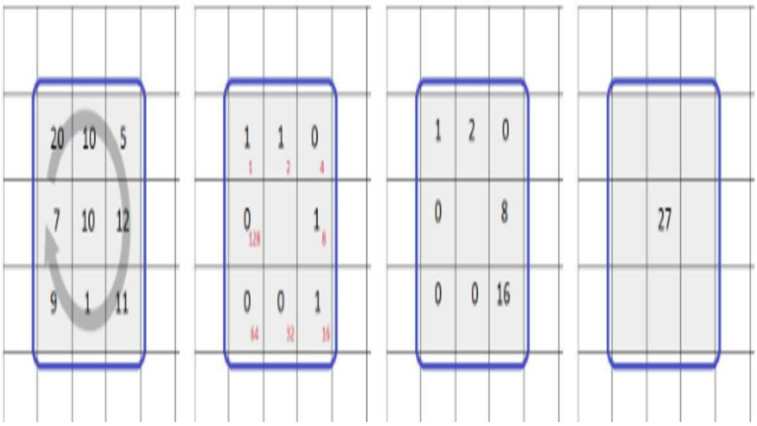

Figure **6.6: Shows calculation of local binary pattern**

— Calculate the interpolation weights and interpolated pixel values.

— Compute the variance matrix using LBP codes which are computed using N sampling points on a circle of radius R and using mapping table

— Calculate LBP Histogram Fourier

$$LBPriu2(P,R) = \sum_{p-1} u(g_i - g_c), ifU(LBP(P,R)) \leqslant 2P+1, otherwise \quad (6.1)$$

— Calculate Linear configuration coefficients

— Estimate optimal weights, associating with intensities of neigboring pixels to linearly reconstruct the central pixel intensity by :

$$E(a_0, ...a_{p-1}) = |g^c - \sum_{p-1} a_i g_i| \quad (6.2)$$

— To minimize the reconstruction error (E(a0 ,.....ap-1)) for each pattern optimal parameters determined by least squares estimation.

6.4 Bag of Feature

Bag-of-features representations have recently become popular for content based image classification owing to their simplicity and good performance. They evolved from texton methods in texture analysis. The basic idea is to treat images as loose collections of independent patches, sampling a representative set of patches from the image, evaluating a visual descriptor vector for each patch independently, and using the resulting distribution of samples in descriptor space as a characterization of the image. The bag-of-words (BoW) model was first used in the context of text categorization (Joachims,

1998; Tong and Koller, 2001). Later it has been adopted to computer vision problems such as image classification and image retrieval (Sivic and Zisserman, 2003). Csurka et al. extracted affine invariant descriptors of image patches and then used vector quantization methods to form the visual words from these descriptors. In another work, Sivic and Zisserman (Sivic and Zisserman, 2003) used a similar approach to form their visual words and applied it to object and scene retrieval in videos. After its introduction to computer vision community, the BoW model has rapidly become a preferred baseline model in object and image classification tasks, and several variations, (Lazebnik et al., 2006) have been proposed.

Our proposed method consists of two major steps : In the first step, a set of code-words is generated by using an unsupervised learning method. In the second step,we represent each pixel or anatomical region with the relative frequencies of their code-words and then use these relative frequencies as an input to recognize the thyroid nodules .

6.5 Transfer Learning

Number of training data is very important to train deep neural network. Unfortunately in medical area, collecting large number of dataset is very challenging task and require to many times. When the number of dataset is not sufficient in each class, we encounter the problem of over-fitting. In order to prevent over-fitting we can augment our dataset by scaling, rotation, transformation of images. An other approach to prevent over-fitting is to use drop out method. Drop out method provide to ignore some of the neurons during training phase which are chosen randomly (Fig. 6.6). In this study we have increase our dataset by noise reduction and we have supported our proposed deep neural network model by drop out model. We used 0.04 drop out values in the fully connected layer.

Alternative approaches for training a deep CNN in the presence of less than required size of a dataset are transfer learning and fine tuning (Huynh et al., 2016). Transfer learning provide to reduce over-fitting in models. Optimization of the hyper-parameters and determining the optimal learning rate of the neural net for different layers are very challenging tasks due to the limited knowledge about the relevance of the large number of architectural and training hyper-parameters. Moreover, the success rate of the transfer learning-based systems is highly dependent on the dataset used for training.

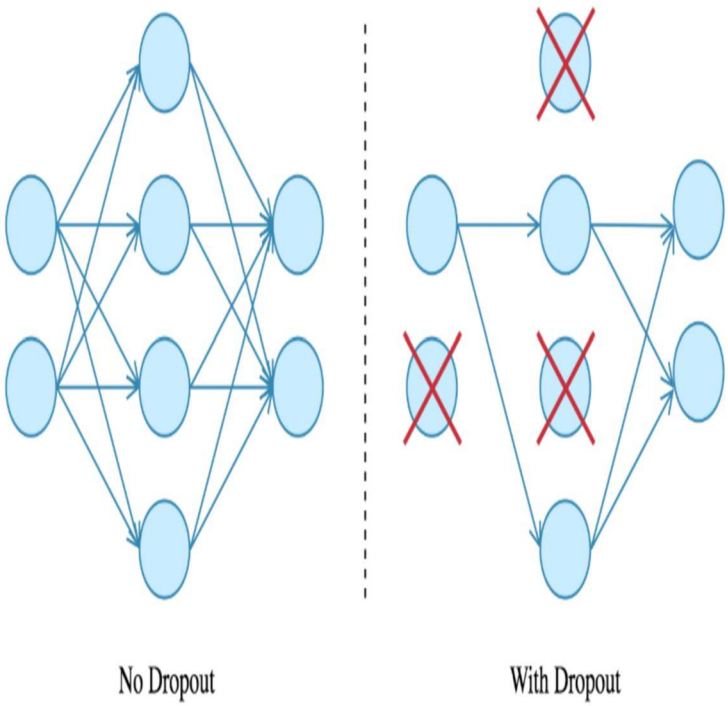

Figure **6.7: Demonstration of drop out method**

In the absence of the knowledge of pre-trained weights of a neural net resembling our dataset (Shin et al., 2016; Ma et al., 2017) , we used AlexNet after fine-tuning certain parameters to classify thyroid nodules. Although we did not assume to get satisfactory results, we applied AlexNet to our dataset for the sake of comparison and to receive a baseline. The success rate of AlexNet was 82.09%.

7 EXPERIMENTAL RESULT

Thyroid gland which is located anteriorly in the neck region of the human body is one of the major hormone secreting glands of the mammalian endocrine system. The thyroid gland consist of follicular cells that produce and store thyroid hormones within the thyroglobulin molecule. The thyroid gland depends on the presence of iodine and tyrosine to achieve its function. The thyroid hormones plays a key role in the regulation of human metabolism and can affect almost every cell in the body. Insufficiency or over production of thyroid hormones lead to pathologies in the gland and results in conditions which affect the whole body. The focus of this study is to discriminate diffuse homogeneous uptake, diffuse non-homogeneous uptake, hyperactive nodule, hypoactive nodule and multi-nodular uptake classes from each other.

The success of a CAD system depends on the performance of the selected feature extraction methods in segmenting thyroid nodules. Proposed CAD system for discrimination of thyroid pathologies from scintigraphic images is based on CNN. Learning capability of CNNs is directly influenced by their architecture. The size and the number of filters used in the convolution layer of CNN has critical role in capturing the discriminative features. The adjustability of a CNN structure offers an endless opportunity to construct many different CNN architectures each of which has a different behavior for a given case.

The focus of this study is to classify thyroid scintigraphy images of different thyroid pathologies which can be defined mainly as diffuse homogeneous uptake, diffuse non-homogeneous uptake, hyperactive nodule, hypoactive nodule and multinodular uptake classes. All of the experiments were carried out on a server having a NVIDIA Geforce GTX Titan X (6 GB on board memeory). The CNN algorithms were performed with the TensorFlow in Keras environment.

We used 10-fold cross-validation method in order to evaluate the stability and reliability of the proposed CNN. The dataset was split into two as 70% training and 30% test sets and test dataset was freed from the training dataset. The selection bias was handled by random sampling of ten cycles which produced different training and test datasets in each cycle of the divided dataset. Different CNN architectures were implemented with TensorFlow using stochastic optimization model of Adam algorithm for training over 150 epochs with a batch size of 32 images (Kingma and Ba, 2014).

The image patches produced with SLS method were given and the success rates of different CNN configurations were evaluated and the CNN configuration which performed the best according to the train-test setup was selected to classify hip types. Our proposed CNN was evaluated with three different approaches. In the beginning the CNN was fed with the original dataset. Secondly the performance of the proposed CNN with the denoised dataset was evaluated. Finally the augmented denoised dataset was fed to the proposed CNN.

Given the original dataset to the proposed CNN configuration the overall accuracy rate was 91.19%.

In the second step, the same CNN configuration was evaluated with the dataset denoised by OBNLM method and the overall accuracy rate increased to 92.82% from 91.19%. The effect of image denoising on the thyroid nodule classification was monitored especially in the hypoactive nodule groups. There was a remarkable increase in differentiation of hyperactive nodule and diffuse non homogenous uptake which increased from 70.08% to 88.73% and 73.17% to 92.97%, respectively. Therefore image denoising increased the classification success of the proposed CNN most probably due to elimination of the negative effect of the speckle noise on the learning capability of the CNN.

It is stated in the literature that the success of a given CNN largely depends on the magnitude of the training dataset. In order to feed the proposed CNN with a larger and a higher quality dataset we proposed to augment our dataset with rotation and scalling . The overall accuracy rate of the proposed CNN was 94.06%. The success rate of the proposed system was 96.07% for homogeneous uptake, 94.08% for multinodular uptake and 92.97% for diffuse non homogenous uptake (Table 7.1). This remarkable increase in the diagnosis capability of the system demonstrates the influence of the higher quality and increased number of dataset on the accuracy rates.

In the literature Singh et al.(Singh and Jindal, 2012) extracted gray level co-occurrence matrix (GLCM) features, and classified thyroid nodules with a success rate of 84.62% based on SVM. Acharya et al. (Acharya et al., 2012) extracted fractal dimension, local binary pattern features to classify thyroid nodules as benign and malignant based on SVM. Although these studies have gained encouraging results, they were mostly based on handcrafted features extracted from images with a series of pre-processing. Ding et al. (Ding et al., 2011) extracted statistical and textural features from thyroid elas-

tograms, and then trained with SVM to detect malignancy of thyroid nodules with a maximum classification accuracy rate of 95.2%. Jinlian et al. proposed a hybrid method for thyroid nodule diagnosis, which was a fusion of two pre-trained convolutional neural networks with different convolutional layers and fully-connected layers. The proposed method was validated on 15,000 ultrasound images and the fusion of the two CNN based models lead to significant performance improvement, with an accuracy of 83.02% (Ma et al., 2017). Classification of the thyroid nodules were achieved with the custom made CNN architecture which produced very similar result with an experienced doctor. In our knowledge, it is the first study to classify scintigraphic images based on deep neural network, local configuration pattern and automatically classification of subclass of thyroid nodules as diffuse homogeneous uptake, diffuse non-homogeneous uptake, hyperactive nodule, hypoactive nodule and multinodular uptake classes. For sake of

Table**7.1: Overall accuracy rates of different methods for the classification of thyroid nodules**

Methods of evaluation	Overall accuracy rate of classification (%)
PHOG evaluated on orginal data set	87.61
Bag of Feature evaluated on orginal data set	85.72
Gray level co-occurrence matrix	86.04
Local Configuration Pattern	88.91
AlexNet evaluated on orginal data set	82.09
Proposed CNN with orginal data set	91.19
Proposed CNN with denoised data set	92.82
Proposed CNN with augmented data set	**94.06**

comparison, we have classified scintigraphic images with the state of art methods like pyramid of histograms of orientation gradients (PHOG), gray level co-occurrence matrix [27], local configuration pattern and bag of feature. All of this methods are type of hand crafted method. PHOG method provide to extract shape features. Local configuration pattern used to extract texture features which is improved method of local binary pattern. Local configuration pattern handle the problem of variance of texture pattern. GLCM method is also kind of texture metod that can extract different kind of texture feature according to determined offset values. There is no proof on the optimal offset values. For this reason we take different offset values and tested the accuracy rate of GLCM features on the training dataset. Then we determined the best GLCM co-occurrence matrix and offset parameters. PHOG was applied to capture the local image and its spatial layout with the parameters, 3 levels of pyramid, 8 orientation bins and in the ranges of [0,360]. 680 shape features were obtained with PHOG method and

Table**7.2: Confusion Matrix of Proposed Convolutional Neural Network**

	Confusion Matrix of Proposed CNN for Thyroid Nodules				
	Homogeneous uptake	Diffuse non-homogeneous uptake	Hyperactive nodule	Hypoactive nodule	Multinodular uptake
Homogeneous uptake	96.07	1.62	2.43	0.65	0.80
Diffuse non homogeneous uptake	5.39	92.97	2.43	0.65	0
Hyperactive nodule	1.4	0	73.17	4.60	0.26
Hypoactive nodul	6.37	1.62	4.87	80.26	3.22
Multinodular uptake	3.43	0.54	4.87	7.89	94.08

84 features were selected with correlation based feature selection method. The BoF was applied to extract 500 codebooks to represent similar hip image patches. The success rate of PHOG and BoF were 85.72% and 87.61% respectively. The overall accuracy rate of GLCM and local configuration pattern are 86.04% and 88.91% respectively (Table 7.2).

The reliability of the system is very important especially in the diagnosis and treatment of medical system. In order to demonstrate reliability of our proposed system we calculated different ratios. Sensitivity (true positive rate) and specificity (true negative rate) demonstrates performance of the proposed system on the classification of thyroid nodules. The sensitivity and specificity rate of our system is 92.86% and 95.87% respectively.

Size of dataset very important to train deep neural network in order to prevent overfitting. In order to handle this problem we tried to increase number of dataset by noise reduction and supported our system by using drop out method. The performance of the system on the augmented dataset and denoised dataset is better than original data set. Because our proposed deep neural network may try to extract meaningful information on the noise. When we eliminated noise by OBNLM method the performance of the system increased to 92.82% from 91.19% (Table 7.2). After combining original dataset with noised reduced thyroid image set, the accuracy rate of system increased to 94.06%. It may be better to increase the dataset with different thyroid images taken by different modality and different hospital for the reliability of the system but this type of study and collecting dataset require a lot of time.

An other approaches in this situation is to use transfer learning. Transfer learning is

one of the most useful method to prevent over-fitting for small size of dataset. After fine tunning of parameters, we tested the performance of AlexNet on the classification of thyroid nodules. The performance of AlexNet was 82.0%. AlexNet was trained on the natural images. Our data set was completely different than natural images. This may be major reason of the low accuracy rate of AlexNet. In the literature we could not found any trained neural network on the medical images.

Classification of the thyroid nodules were achieved with the custom made CNN architecture which produced very similar result with an experienced doctor. In our knowledge, it is the first study to classify scintigraphic images based on deep neural network, local configuration pattern and automatically classification of subclass of thyroid nodules as diffuse homogeneous uptake, diffuse non-homogeneous uptake, hyperactive nodule, hypoactive nodule and multi-nodular uptake classes.

8 CONCLUSION

Computer aided diagnosis systems are a very important tool in the decision making before the treatment. This study describes a fully automatic computer aided diagnosis system for thyroid nodules based on statistical level set and CNN methods, especially helpful for nuclear medicine practitioners, endocrinologist and thyroid surgeons. In this study all images were successfully segmented by SLS method to feed custom made CNN in order to recognize thyroid nodules. SLS method transformed images to another domain which provides to determine each object with multiple Gaussian distribution. Segmented thyroid nodules based on SLS model were given to proposed deep CNN architecture as an input. CNN provided to automatically extract features from scintigraphic image patches that contained anatomical structures of thyroid gland and nodules. The success rate of CNN is highly dependent to the quality and the size of training dataset. Original dataset was used to train different CNN architectures to decide the most relevant CNN architecture. Selected CNN architectures were tested on the original dataset and compared to noise reduced dataset based on OBNLM method. Noise reduction based on OBNLM method increased the segmentation and classification results probably due to reduction of speckle noise which provided a better segmentation of anatomical regions and prevented CNN to extract meaningful information from the false signal. We increased number of dataset by combining original dataset and noise reduced thyroid images to increase performance of proposed CAD system. After augmentation of dataset classification success of the proposed system increased to desired level. We compared our system with state of art methods like GLCM, LCP, bag of feature. Transfer learning was applied to determine the baseline of CAD system. As a result the proposed CNN was more successful than handcrafted local shape and texture feature methods and transfer learning. Our proposed CNN based diagnosis system is very promising to assist nuclear medicine practitioners, endocrinologist and surgeons in decision making. Our study demonstrates the impact of reducing noise in the classification of scintigraphic images using the OBNLM method. The drawback of this study is the size of the dataset. A larger quantity of data would further improve the training process and could increase the success of our proposed CNN. The close similarity of the results of our proposed system to those of an experienced expert is very promising for its future use in the clinical environment. Our future work is to collect different thyroid nodules from different machines and test the success of classification thyroid nodules.

REFERENCES

Acharya, U. R., Sree, S. V., Krishnan, M. M. R., Molinari, F., Garberoglio, R. and Suri, J. S. (2012). Non-invasive automated 3d thyroid lesion classification in ultrasound : a class of thyroscan^{TM} systems, *Ultrasonics* **52**(4) : 508–520.

Anthimopoulos, M., Christodoulidis, S., Ebner, L., Christe, A. and Mougiakakou, S. (2016). Lung pattern classification for interstitial lung diseases using a deep convolutional neural network, *IEEE transactions on medical imaging* **35**(5) : 1207–1216.

Arevalo, J., González, F. A., Ramos-Pollán, R., Oliveira, J. L. and Lopez, M. A. G. (2016). Representation learning for mammography mass lesion classification with convolutional neural networks, *Computer methods and programs in biomedicine* **127** : 248–257.

Bai, Y., Guo, L., Jin, L. and Huang, Q. (2009). A novel feature extraction method using pyramid histogram of orientation gradients for smile recognition, *Image Processing (ICIP), 2009 16th IEEE International Conference on*, IEEE, pp. 3305–3308.

Bosch, A., Zisserman, A. and Munoz, X. (2007). Representing shape with a spatial pyramid kernel, *Proceedings of the 6th ACM international conference on Image and video retrieval*, ACM, pp. 401–408.

Chan, T. F. and Vese, L. A. (2001). Active contours without edges, *IEEE Transactions on image processing* **10**(2) : 266–277.

Chen, H., Ni, D., Qin, J., Li, S., Yang, X., Wang, T. and Heng, P. A. (2015). Standard plane localization in fetal ultrasound via domain transferred deep neural networks, *IEEE journal of biomedical and health informatics* **19**(5) : 1627–1636.

Corvilain, B., Van Sande, J., Dumont, J. E., Bourdoux, P. and Ermans, A. M. (1998). Autonomy in endemic goiter, *Thyroid* **8**(1) : 107–113.

Coupé, P., Hellier, P., Kervrann, C. and Barillot, C. (2009). Nonlocal means-based speckle filtering for ultrasound images, *IEEE transactions on image processing* **18**(10) : 2221–2229.

D'Andrea, V., Cantisani, V., Catania, A., Di Matteo, F. M., Sorrenti, S., Greco, R., Kyriacos, K., Menichini, G., Marotta, E., De Stefano, M. et al. (2009). Thyroid tissue remnants after "total thyroidectomy", *Il Giornale di chirurgia* **30**(8/9) : 339–344.

Deselaers, T., Pimenidis, L. and Ney, H. (2008). Bag-of-visual-words models for adult image classification and filtering, *Pattern Recognition, 2008. ICPR 2008. 19th International Conference on*, IEEE, pp. 1–4.

Dhall, A., Asthana, A., Goecke, R. and Gedeon, T. (2011). Emotion recognition using phog and lpq features, *Automatic Face & Gesture Recognition and Workshops (FG 2011), 2011 IEEE International Conference on*, IEEE, pp. 878–883.

Ding, J., Cheng, H., Ning, C., Huang, J. and Zhang, Y. (2011). Quantitative measurement for thyroid cancer characterization based on elastography, *Journal of Ultrasound in Medicine* **30**(9) : 1259–1266.

Ghasemi, A. and Safabakhsh, R. (2012). A real-time multiple vehicle classification and tracking system with occlusion handling, *Intelligent Computer Communication and Processing (ICCP), 2012 IEEE International Conference on*, IEEE, pp. 109–115.

Ghesu, F. C., Krubasik, E., Georgescu, B., Singh, V., Zheng, Y., Hornegger, J. and Comaniciu, D. (2016). Marginal space deep learning : efficient architecture for volumetric image parsing, *IEEE transactions on medical imaging* **35**(5) : 1217–1228.

Hegedüs, L. (2004). The thyroid nodule, *New England Journal of Medicine* **351**(17) : 1764–1771.

Huynh, B., Drukker, K. and Giger, M. (2016). Mo-de-207b-06 : Computer-aided diagnosis of breast ultrasound images using transfer learning from deep convolutional neural networks, *Medical Physics* **43**(6) : 3705–3705.

Iakovidis, D. K., Savelonas, M. A., Karkanis, S. A. and Maroulis, D. E. (2007). A genetically optimized level set approach to segmentation of thyroid ultrasound images, *Applied Intelligence* **27**(3) : 193–203.

Joachims, T. (1998). Text categorization with support vector machines : Learning with many relevant features, *European conference on machine learning*, Springer, pp. 137–142.

Keramidas, E. G., Iakovidis, D. K., Maroulis, D. and Karkanis, S. (2007). Efficient and effective ultrasound image analysis scheme for thyroid nodule detection, *International Conference Image Analysis and Recognition*, Springer, pp. 1052–1060.

Keramidas, E. G., Maroulis, D. and Iakovidis, D. K. (2012). Tnd : a thyroid nodule detection system for analysis of ultrasound images and videos, *Journal of medical systems* **36**(3) : 1271–1281.

Kingma, D. and Ba, J. (2014). Adam : A method for stochastic optimization, *arXiv preprint arXiv :1412.6980* .

Kirsten, D. (2000). The thyroid gland : physiology and pathophysiology, *Neonatal Network* **19**(8) : 11–26.

Koundal, D., Gupta, S. and Singh, S. (2016). Automated delineation of thyroid nodules in ultrasound images using spatial neutrosophic clustering and level set, *Applied Soft Computing* **40** : 86–97.

Lazebnik, S., Schmid, C. and Ponce, J. (2006). Beyond bags of features : Spatial pyramid matching for recognizing natural scene categories, *null*, IEEE, pp. 2169–2178.

Ma, J., Luo, S., Dighe, M., Lim, D.-J. and Kim, Y. (2010). Differential diagnosis of thyroid nodules with ultrasound elastography based on support vector machines, *Ultrasonics Symposium (IUS), 2010 IEEE*, IEEE, pp. 1372–1375.

Ma, J., Wu, F., Zhu, J., Xu, D. and Kong, D. (2017). A pre-trained convolutional neural network based method for thyroid nodule diagnosis, *Ultrasonics* **73** : 221–230.

Margeta, J., Criminisi, A., Cabrera Lozoya, R., Lee, D. C. and Ayache, N. (2015). Fine-tuned convolutional neural nets for cardiac mri acquisition plane recognition, *Computer Methods in Biomechanics and Biomedical Engineering : Imaging & Visualization* pp. 1–11.

Maroulis, D. E., Savelonas, M. A., Iakovidis, D. K., Karkanis, S. A. and Dimitropoulos, N. (2007). Variable background active contour model for computer-aided delineation of nodules in thyroid ultrasound images, *IEEE Transactions on Information Technology in Biomedicine* **11**(5) : 537–543.

Moreno-Reyes, R., Kyrilli, A., Lytrivi, M., Bourmorck, C., Chami, R. and Corvilain, B. (2016). Is there still a role for thyroid scintigraphy in the workup of a thyroid nodule in the era of fine needle aspiration cytology and molecular testing ?, *F1000Research* **5**.

Ozdemir, D., Cuhaci, F. N., Ozdemir, E., Aydin, C., Ersoy, R., Turkolmez, S. and Cakir, B. (2016). The role of postoperative tc-99m pertechnetate scintigraphy in estimation of remnant mass and prediction of successful ablation in patients with differentiated thyroid cancer, *Nuclear medicine communications* **37**(6) : 640–645.

Paragios, N. and Deriche, R. (2000). Geodesic active contours and level sets for the detection and tracking of moving objects, *IEEE Transactions on pattern analysis and machine intelligence* **22**(3) : 266–280.

Salvatori, M., Raffaelli, M., Castaldi, P., Treglia, G., Rufini, V., Perotti, G., Lombardi, C. P., Rubello, D., Ardito, G. and Bellantone, R. (2007). Evaluation of the surgical completeness after total thyroidectomy for differentiated thyroid carcinoma, *European Journal of Surgical Oncology (EJSO)* **33**(5) : 648–654.

Sarkar, S. D. (2006). Benign thyroid disease : what is the role of nuclear medicine ?, *Seminars in nuclear medicine*, Vol. 36, Elsevier, pp. 185–193.

Savelonas, M. A., Iakovidis, D. K., Legakis, I. and Maroulis, D. (2009). Active contours guided by echogenicity and texture for delineation of thyroid nodules in ultrasound images, *IEEE Transactions on Information Technology in Biomedicine* **13**(4) : 519–527.

Shin, H.-C., Roth, H. R., Gao, M., Lu, L., Xu, Z., Nogues, I., Yao, J., Mollura, D. and Summers, R. M. (2016). Deep convolutional neural networks for computer-aided detection : Cnn architectures, dataset characteristics and transfer learning, *IEEE transactions on medical imaging* **35**(5) : 1285–1298.

Singh, N. and Jindal, A. (2012). Ultra sonogram images for thyroid segmentation and texture classification in diagnosis of malignant (cancerous) or benign (non-cancerous) nodules, *International Journal of Engineering and Innovative Technology (IJEIT)* **1**(5) : 202–206.

Sivic, J. and Zisserman, A. (2003). Video google : A text retrieval approach to object matching in videos, *null*, IEEE, p. 1470.

Spratt, D. E., Zaki, B. I., Franc, B. L., Hartford, A. C. and Osborne, J. R. (2016). Acr practice parameter for the performance of therapy with unsealed radiopharmaceutical sources, *Clinical nuclear medicine* **41**(2) : 106–117.

Tajbakhsh, N., Gotway, M. B. and Liang, J. (2015). Computer-aided pulmonary embolism detection using a novel vessel-aligned multi-planar image representation and

convolutional neural networks, *International Conference on Medical Image Computing and Computer-Assisted Intervention*, Springer, pp. 62–69.

Tong, S. and Koller, D. (2001). Support vector machine active learning with applications to text classification, *Journal of machine learning research* **2**(Nov) : 45–66.

Tsantis, S., Dimitropoulos, N., Cavouras, D. and Nikiforidis, G. (2006). A hybrid multiscale model for thyroid nodule boundary detection on ultrasound images, *Computer methods and programs in biomedicine* **84**(2-3) : 86–98.

Vorländer, C., Wolff, J., Saalabian, S., Lienenlüke, R. H. and Wahl, R. A. (2010). Real-time ultrasound elastography—a noninvasive diagnostic procedure for evaluating dominant thyroid nodules, *Langenbeck's archives of surgery* **395**(7) : 865–871.

Wang, X.-F., Huang, D.-S. and Xu, H. (2010). An efficient local chan–vese model for image segmentation, *Pattern Recognition* **43**(3) : 603–618.

Wu, K., Chen, X. and Ding, M. (2014). Deep learning based classification of focal liver lesions with contrast-enhanced ultrasound, *Optik-International Journal for Light and Electron Optics* **125**(15) : 4057–4063.

Yu, L., Guo, Y., Wang, Y., Yu, J. and Chen, P. (2016). Segmentation of fetal left ventricle in echocardiographic sequences based on dynamic convolutional neural networks, *IEEE Transactions on Biomedical Engineering* .

Zhang, J., Wang, C. and Cheng, Y. (2015). Comparison of despeckle filters for breast ultrasound images, *Circuits, Systems, and Signal Processing* **34**(1) : 185–208.

Zhang, K., Zhang, L., Lam, K.-M. and Zhang, D. (2016). A level set approach to image segmentation with intensity inhomogeneity, *IEEE transactions on cybernetics* **46**(2) : 546–557.

Zhang, K., Zhang, L. and Zhang, S. (2010). A variational multiphase level set approach to simultaneous segmentation and bias correction, *2010 IEEE International Conference on Image Processing*, IEEE, pp. 4105–4108.

Zhang, Q., Xiao, Y., Dai, W., Suo, J., Wang, C., Shi, J. and Zheng, H. (2016). Deep learning based classification of breast tumors with shear-wave elastography, *Ultrasonics* **72** : 150–157.

Zhao, C., Zhang, X., Zhang, B., Dang, Q. and Lian, J. (2013). Driver's fatigue expressions recognition by combined features from pyramid histogram of oriented gradient

and contourlet transform with random subspace ensembles, *IET Intelligent Transport Systems* **7**(1) : 36–45.

Zhu, C., Zheng, T., Kilfoy, B. A., Han, X., Ma, S., Ba, Y., Bai, Y., Wang, R., Zhu, Y. and Zhang, Y. (2009). A birth cohort analysis of the incidence of papillary thyroid cancer in the united states, 1973–2004, *Thyroid* **19**(10) : 1061–1066.

APPENDIX A PROOF OF SOME THEOREM

This is appendix text.

BIOGRAPHICAL SKETCH

Post-Doc Ph.D. 2017-2019 École nationale supérieure de techniques avancées (ENSTA) Unité d'Informatique et Ingénierie des Systèmes (BRIDGES European Union Horizon 2020 program)

Ph.D. 2009- 2015 Yildiz Technical University, Department of Computer Engineering, Turkey

M.S. 2007-? Galatasaray University, Department of Industrial Engineering, Turkey

M.S. 2006-2008 Halic University, Department of Computer Engineering, Istanbul, Turkey

B.A. 2000-2005 İstanbul Kultur University, Department of Computer Engineering, Turkey

B.A. 2000-2006 İstanbul Kultur University, Department of Industrial Engineering, Turkey

Lycee 1997-2000 Lycée Clemenceau, France (one year) and Burak Bora, Istanbul, Turkey

College 1994-1997 College Romain Rolland, France

PUBLICATIONS

— Sezer, A., Sezer, H. B., Albayrak, S. Hermite-based texture feature extraction for classification of humeral head in proton density-weighted MR images. Neural Computing and Applications, 1-13.

— Sezer, A., Sezer, H. B., Albayrak, S. (2015). Segmentation of bone with region based active contour model in PD weighted MR images of shoulder. Computational and mathematical methods in medicine, 2015.

Method of Normal and Edematous Humeral Head from PD Weighted MR Images Based on GLCM Texture Features. International journal of advance computational engineering and networking volume 3 issue 6

— Sezer, A., Sezer, H. B., Convolutional Neural Network Based Diagnosis of Bone Pathologies of Proximal Humerus. Neurocomputing (accepted 20 November 2018)

— Sezer, A., Sezer, H. B., Computer based diagnosis of hip dysplasia from Graf's hip ultrasonography. Applied Soft Computing. (under review since 2017)

— Sezer, A., Sezer, H. B., Deep Convolutional Neural Network Based Automatic Classification of Neonatal Hip Ultrasound Images. Ultrasonics (under review)

— Capsule Network based Classification of Rotator Cuff Tears from MRI, Magnetic Resonance Imaging (under review)

— Sezer, A., Çekmez, U. (2017, May). Cells classification with deep learning. In Signal Processing and Communications Applications Conference (SIU), 2017 25th (pp. 1-4). IEEE.

— Sezer, A., Sigirci, I. O., Sezer, H. B. (2017, May). Shoulder lesion classification using shape and texture features via composite kernel. In Signal Processing and Communications Applications Conference (SIU), 2017 25th (pp. 1-4). IEEE.

— Sezer, A., Sezer, H. B. (2017, May). Bag of feature based classification of bone from MR images. In Signal Processing and Communications Applications Conference (SIU), 2017 25th (pp. 1-4). IEEE.

— Sezer Aysun, Hasan Basri Sezer, Songul Albayrak (2015). Classification of bone pathologies with finite discrete shearlet transform based shape descriptors. The fifth International Conference on Image Processing Theory, Tools and Applications IPTA'15

— Sezer Aysun, Hasan Basri Sezer, Songul Albayrak (2015). Segmentation of humeral head from axial proton density weighted shoulder MR images. Tenth International Symposium on Medical Information Processing and Analysis. International Society for Optics and Photonics.

— Sezer, Aysun, Hasan Basri Sezer, Songul Albayrak. (2014). Segmentation of humeral head from MR slices. Signal Processing and Communications Applications Conference (SIU), 2014 22nd. IEEE.